
CNN LEGO: Disassembling and Assembling Convolutional Neural Network

Jiacong Hu
Zhejiang University
jiaconghu@zju.edu.cn

Jing Gao
Zhejiang University
jinggao@zju.edu.cn

Zunlei Feng
Zhejiang University
zunleifeng@zju.edu.cn

Lechao Cheng
Zhejiang University
chenglc@zju.edu.cn

Jie Lei
Zhejiang University Of Technology
jasonlei@zjut.edu.cn

Hujun Bao
Zhejiang University
bao@cad.zju.edu.cn

Mingli Song
Zhejiang University
brooksong@zju.edu.cn

Abstract

Convolutional Neural Network (CNN), which mimics human visual perception mechanism, has been successfully used in many computer vision areas. Some psychophysical studies show that the visual perception mechanism synchronously processes the form, color, movement, depth, etc., in the initial stage [11, 28] and then integrates all information for final recognition [47]. What's more, the human visual system [28] contains different subdivisions or different tasks. Inspired by the above visual perception mechanism, we investigate a new task, termed as Model Disassembling and Assembling (MDA-Task), which can disassemble the deep models into independent parts and assemble those parts into a new deep model without performance cost like playing LEGO toys. To this end, we propose a feature route attribution technique (FRAT) for disassembling CNN classifiers in this paper. In FRAT, the positive derivatives of predicted class probability w.r.t. the feature maps are adopted to locate the critical features in each layer. Then, relevance analysis between the critical features and preceding/subsequent parameter layers is adopted to bridge the route between two adjacent parameter layers. In the assembling phase, class-wise components of each layer are assembled into a new deep model for a specific task. Extensive experiments demonstrate that the assembled CNN classifier can achieve close accuracy with the original classifier without any fine-tune, and excess original performance with one-epoch fine-tune. What's more, we also conduct massive experiments to verify the broad application of MDA-Task on model decision route visualization, model compression, knowledge distillation, transfer learning, incremental learning, and so on.

1 Introduction

Convolutional neural networks (CNN), the mainstream deep learning model architecture, has achieved milestone breakthrough in the computer vision area. However, the well-known 'black-box' characteristic of CNN has limited its further research and application. CNN was initially inspired by the concept of receptive field in the biological visual system [19]. The biological visual information processing system consists of visual senses, visual pathways and multi-level visual centers that enable the generation, transmission and processing of visual information [28].

There have been many works [11, 28, 47] that focus on exploring the mechanisms of the biological visual information processing systems. The psychophysical studies conducted by Livingstone et al. [28] and Essen et al. [11] show that visual information such as form, color, movement, and depth are synchronously processed in the primary visual cortical areas. In the latter half of the visual information processing, different visual information processed by the primary visual cortical areas are integrated for the final recognition [47]. Furthermore, Livingstone et al. [28] have verified that the intermediate visual cortex neural mechanisms are composed of relatively independent subdivisions.

Some works [10, 29, 31, 32, 40, 44] try to visualize significant layers and neurons of CNN models, which shows that form, color, texture, edge features are processed by different convolutional kernels in the low-level of CNN, and the class-aware features occur in the high-level of CNN. The above phenomena indicate that the feature processing mechanism of CNN is similar to the parallel processing mechanism [11, 28] and information integration theory [47] of the biological visual systems.

The subdivisions of the visual system raise a question: *Are the deep models also composed of different subsystems?* Unfortunately, few works have investigated the subsystem in deep models until now. In this paper, we investigate a novel task, termed as Model Disassembling and Assembling (MDA-Task), in response to the above subsystem question. For MDA-Task, based on the subsystem consumption, the deep models are expected to be disassembled and assembled without performance cost like playing LEGO toys. The MDA-Task is supposed to be appropriate for existing deep learning model such as CNN, GCN, GNN, RNN, Transformer, and et al.

To this end, we focus on disassembling and assembling the CNN classifier in this paper. The essence of disassembling the CNN classifier is discovering the inherent feature route associated with the specific class from a trained CNN classifier. The feature route discovery is split into two steps: critical feature attribution and bridging the route between two adjacent layers, which can build the whole feature route of a CNN classifier.

In the feature attribution step, the positive first-order derivatives of predict class probability w.r.t the feature maps are adopted to attribute the critical features. Experiments results show that each class is only associated with some fixed feature maps, as shown in Fig. 2, which is the fundamental support of the following research. Then, the relevance analysis between the critical features and preceding/subsequent parameter layers is conducted to bridge the route between two adjacent parameter layers.

In the assembling stage, we devise a simple alignment padding strategy for assembling class-aware components of the same or different models through padding empty kernels for each convolutional filter, which ensures that all filters in each layer have the same number of kernels.

Our contribution is therefore introducing the new MDA-Task, with the aim to disassemble and assemble deep models without performance loss like playing LEGO toys, which is inspired by the subdivision of the visual system [28]. To this end, we put forward the first model disassembling and assembling framework for investigating the sub-classification system of the CNN class. In disassembling stage, the feature route attribution technique (FRAT) is proposed for attributing the critical features in each layer and bridging the feature route between the two adjacent layers. Extensive experiments are conducted to verify the effectiveness of the proposed MDA-Task and FRAT that assembled new classifier can achieve close even better performance than the original classifier. What's more, we further verify the broad application of MDA-Task on various tasks, such as decision route visualization, model compression, knowledge distillation, and so on.

2 Related Work

As far as we know, no work investigates the Model Disassembling and Assembling Task (MDA-Task). In this section, we summarize and analyze some closely related techniques to the MDA-Task and the proposed feature route attribution technique.

2.1 Deep Feature Attribution

Existing deep feature attribution methods can be divided into three types: perturbation-based methods [26, 51, 53, 54], activation-based methods [8, 30, 48, 52], and back-propagation-based methods [1, 2, 3, 12, 21, 38, 39, 41, 43, 45].

Perturbation-based methods [26, 51, 53, 54] directly compute the importance of an input feature by measuring the output differences with the original features and the perturbed (altering, removing, or masking) feature as input.

For the activation based method, Simonyan et al. [40] adopted the activation maximization to build the saliency maps for visualizing convolutional networks. Zhou et al. [52] proposed Class Activation Mapping (CAM), which computes a weighted sum of the feature maps of the last convolutional layer to obtain the class activation maps, to visualize the predicted class scores on any given image, highlighting the discriminative object parts detected by the CNN. Wang et al. [48] proposed the score-CAM using the increase in confidence as the weight of each activation map, which is a novel CAM variant. Naidu and Michael [30] introduced an enhanced visual explanation for visual sharpness called SS-CAM, which uses the smooth operation (adding noise into the feature map or the input image) to produce centralized localization of object features within an image. Desai and Ramaswamy [8] proposed the Ablation-CAM that uses ablation analysis to determine the importance (weights) of individual feature map units w.r.t. time-consuming class.

For the backpropagation-based method, Baehrens et al. [3] first applied the first-order derivative of the predict class w.r.t. the input to explain classification decisions of the Bayesian classification task. Furthermore, Simonyan et al. [41] extended the same technique into the CNN classification network to extract class-aware saliency maps. Sundararajan et al. [45] took the (signed) partial derivatives of the output w.r.t the input and multiplied them with the input itself (i.e., $\text{Gradient} \times \text{Input}$), which improves the sharpness of the attribution maps. Shrikumar et al. [39] computed the average gradient while the input varies along a linear path from a baseline, which is defined by the user and often chosen to be zero, to the initial input (i.e., Integrated Gradients). Shrikumar et al. [38] recently proposed DeepLift that decomposes the output prediction of a neural network on a specific input by backpropagating the contributions of all neurons in the network to every feature of the input. Bach et al. [2] and Feng et al. [12] proposed the Layerwise Relevance Propagation (LRP), which decomposes the predicted class probability into sums of feature and pixel relevance score. The final relevance visualizes the contribution of single pixels to the prediction. Kindermans et al. [21] showed that the original LRP rules were equivalent within a scaling factor to the $\text{gradient} \times \text{input}$. Feng et al. [13] summed the first-order derivative of predicted probability w.r.t. the feature map to discriminate the related and unrelated convolutional filters for a specific class, which are used for diagnosing and treating CNN classifiers.

Furthermore, above $\text{Gradient} \times \text{Input}$, ϵ -LRP, Integrated Gradients and DeepLIFT (rescale) are analyzed from theoretical and practical perspectives in [1], which shows that these four methods, despite their different formulation, are firmly related, proving conditions of equivalence or approximation between them. It's noticeable that the gradient w.r.t. the feature map is also adopted to locate the important features in the paper. Unlike the above methods, we adopt the attributed important features to bridge the feature route between two adjacent layers. What's more, only the positive gradient is adopted to bridge the feature route in our method. The validity of the positive gradient is verified by detailed experiments and analysis in ablation study on derivatives (Section 6.7).

2.2 Decision Route Approximation

The core of decision route approximation is to adopt explainable modules such as simple linear modules to approximate the output of a deep model. Ribeiro et al. [35] proposed LIME that explains the predictions of any classifier by learning an interpretable linear model locally around the prediction. Guo et al. [15] extended the LIME into the RNN model. Guidotti et al. [14] proposed LORE, which first learns a local interpretable predictor on a synthetic neighborhood generated by a genetic algorithm and then derives from the logic of the local interpretable predictor a meaningful explanation. Ribeiro et al. [34, 36] proposed an if-then rules-based model explanation method anchor-LIME, where an anchor explanation is a rule that sufficiently anchors the prediction locally. Bastani et al. [4], and Lei et al. [25] adopted the explainable random forests to approximate the 'black-box' deep model. Recently, Chen et al. [7], and Xue et al. [50] incorporated the tree architecture into the CNN classifier, which contributes to sparse connection and better accuracy. Unlike the above methods, the proposed model disassembling aims to discover the inherent feature route of the trained CNN classifier for the specific class, which does not need the assistance of simple explainable modules.

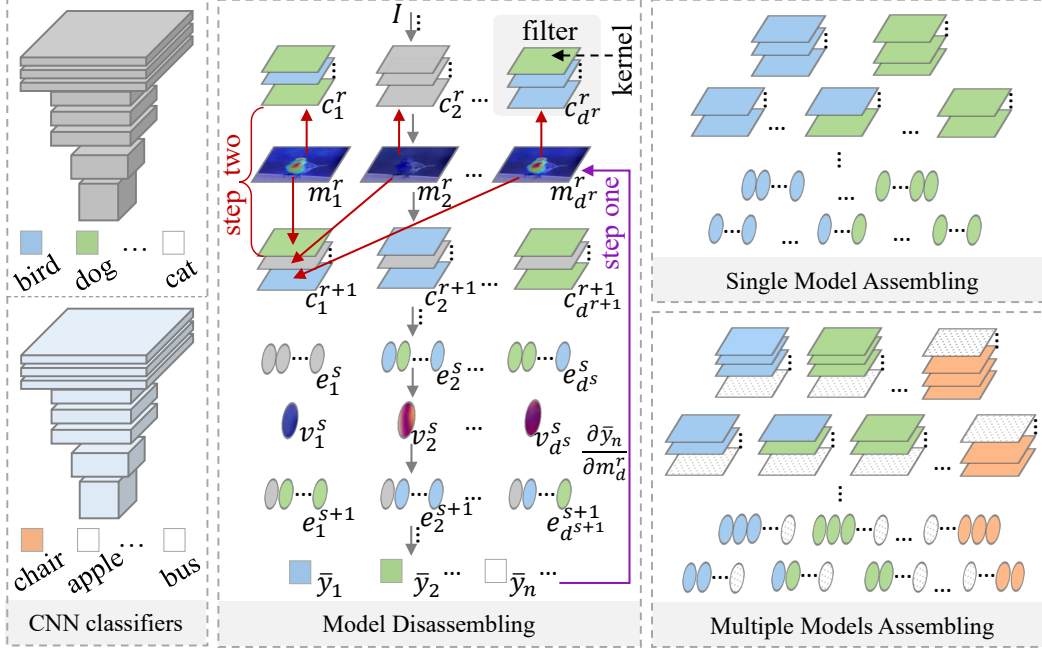


Figure 1: The framework of disassembling and assembling CNN classifier. The model disassembling contains two steps: critical feature attribution (step one) and layer component bridging (step two). For an input image I , the CNN classifier, composed of multiple convolutional layers and linear connection layers, predicts its probability as \bar{y}_n . The convolutional filter in the r -th layer is denoted as $c_d^r \in \mathbf{R}^{h^r * w^r * d^{r-1}}$, where h^r , w^r , and d^{r-1} denote the height, width, and the number of convolutional kernels, respectively. Each filter c_d^r is composed of d^{r-1} kernels $\{k_d^r\}_{d=1}^{d^{r-1}}$. In step one, the positive derivative $\frac{\partial \bar{y}_n}{\partial m_d^r}$ of \bar{y}_n w.r.t. the d -th feature map m_d^r is adopted to locate the critical features for the n -th class. In step two, the derivative value of $\frac{\partial \bar{y}_n}{\partial m_d^r}$ determines whether the d -th filter c_d^r and the d -th kernel k_d^{r+1} of each filter in the $(r+1)$ -th layer are relevant with the n -th class, which bridges the feature route between the r and $(r+1)$ layers for the n -th class. A simple alignment padding strategy is devised in the assembling phase to assemble class-aware components of single or multiple models through padding empty kernels for convolutional filters in each layer.

3 Model Disassembling and Assembling Task

The definition of Model Disassembling and Assembling Task (MDA-Task) is given as follows. Assumed that there is a trained deep model \mathcal{M}^1 of task T^1 composed of N sub-tasks $\{t_1^1, t_2^1, \dots, t_n^1, \dots, t_N^1\}$, the goal of model disassembling is discovering the inherent feature route $\mathcal{M}^1[t_n^1]$ for the specific sub-task t_n^1 . The discovered feature route $\mathcal{M}^1[t_n^1]$ should contain important components relevant to the sub-task t_n^1 . In other words, the disassembled components $\mathcal{M}^1[t_n^1]$ are supposed to maintain the intact capacity of the sub-task t_n^1 and have no redundant capacity for other sub-tasks. With disassembled components $\mathcal{M}^1[t_1^1, t_2^1, \dots, t_n^1, \dots, t_N^1]$ and $\mathcal{M}^2[t_1^2, t_2^2, \dots, t_{n'}^2, \dots, t_{N'}^2]$, the assembled new model $\mathcal{M}^{new}[t_{n_1}^1, \dots, t_{n_2}^1, t_{n'_1}^2, \dots, t_{n'_2}^2]$ should possess the intact and integrated capacity for the sub-tasks $\{t_{n_1}^1, \dots, t_{n_2}^1\}$ and $\{t_{n'_1}^2, \dots, t_{n'_2}^2\}$.

The MDA-Task is applicable for existing deep learning models such as CNN, GCN, GNN, RNN, Transformer, etc. This paper focuses on investigating the MDA-Task on the CNN classifiers.

4 CNN Model Disassembling

4.1 How to disassemble a CNN classifier?

For a trained CNN classifier, the essence of model disassembling is to discover the inherent feature route associated with a specific class and disassemble those parameter components from the original CNN classifier.

As mentioned earlier, different features such as form, color, texture, and edge features are processed by different convolutional kernels in the low level of CNN [10, 29, 31, 32, 40, 44], which is similar to the parallel processing mechanism [11, 28]. This paper first tries to locate those critical and independent features. Then, adopting those critical features to locate the corresponding processing convolutional filters and bridge the feature routes between the parameter components of the preceding and following layers. With the discovered critical features and feature routes, the whole feature route for the specific class can be easily built. Thus, the whole disassembling process is divided into two steps: feature attribution and layer component bridging. Fig. 1 shows the disassembling framework for the CNN classifier.

4.2 Feature Attribution

For the CNN classifier, an input image I will go through multiple convolutional layers and linear connection layers, then is predicted as the probability \bar{y}_n for the n -th class. In the following description, the convolutional filters of the r -th layer are denoted as $\{c_d^r \in \mathbf{R}^{h^r * w^r * d^{r-1}}\}_{d=1}^{d^r}$, where h^r , w^r , d^r , d^{r-1} denote the height, width, number, kernel number of the convolutional filter c_d^r , respectively. Each convolutional filter c_d^r is composed of d^{r-1} kernels $\{k_d^r\}_{d=1}^{d^{r-1}}$. It is worth noting that the number of filters for $(r-1)$ -th layer is equal to the number of kernels for each filter in the r -th layer due to the convolution operation. For simplicity, we omit the descriptions about operations that do not change the feature dimension, including batch norm, dropout, activation function, pooling, etc.

As shown in Fig. 1, the CNN classifier comprises multiple convolutional layers and linear connection layers. Each convolutional layer contains d^r convolutional filters $\{c_d^r\}_{d=1}^{d^r}$, where each filter c_d^r is composed of d^{r-1} kernels $\{k_d^r\}_{d=1}^{d^{r-1}}$. Each linear connection layer contains d^s filters $\{e_d^s\}_{d=1}^{d^s}$, where each filter e_d^s is composed of d^{s-1} neurons. For the convolution operation in r -th layer, the feature map m_d^r is calculated as follows:

$$m_d^r = f(c_d^r \otimes \{m_1^{r-1}, m_2^{r-1}, \dots, m_{d^{r-1}}^{r-1}\}), \quad (1)$$

where \otimes denotes the convolutional operation.

Similarly, for calculating operation in the linear layer, the output response value v_d^s is calculated as follows:

$$v_d^s = f(e_d^s \ominus \{v_1^{s-1}, v_2^{s-1}, \dots, v_{d^{s-1}}^{s-1}\}), \quad (2)$$

where \ominus denotes the linear operation.

Then, the final class prediction probability \bar{y}_n is calculated as follows:

$$\bar{y}_n = F(\{v_1^s, v_2^s, \dots, v_{d^s}^s\}), \quad (3)$$

where F denotes the final linear mapping operation.

For the feature maps $\{m_1^r, m_2^r, \dots, m_{d^r}^r\}$, the first-order derivative $(\bar{y}_n)'_{m_d^r}$ of the predicted class probability \bar{y}_n w.r.t. the feature map m_d^r is calculated as follows:

$$(\bar{y}_n)'_{m_d^r} = \frac{\partial \bar{y}_n}{\partial m_d^r}. \quad (4)$$

For the first-order derivatives $(\bar{y}_n)'_{m_d^r}$, only the positive values are summed into a response value $a_d^{n,r}$ as follows:

$$a_d^{n,r} = \uplus \left| \frac{\partial \bar{y}_n}{\partial m_d^r} \right|^+, \quad (5)$$

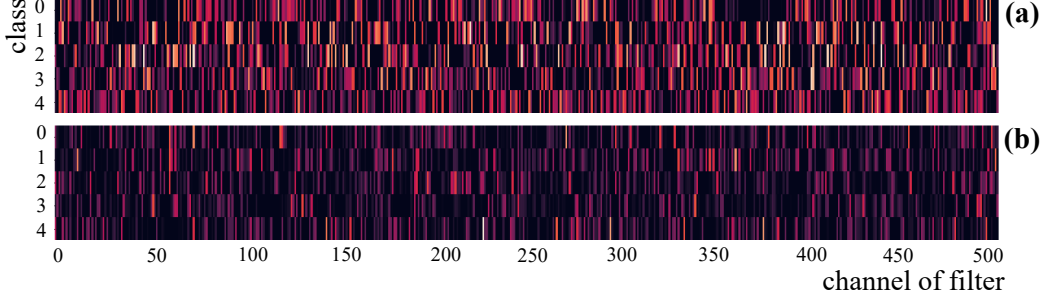


Figure 2: The statistical correlation diagram between all classes and the convolutional filters (a) / linear filters (b) in the 13-th convolution layer / 2-nd linear layer of VGG-16 ON CIFAR-10-A. The bright and dark colors indicate high and low correlation, respectively.

where $\left| \frac{\partial \bar{y}_n}{\partial m_d^r} \right|^+$ denotes taking positive values in the matrix $\frac{\partial \bar{y}_n}{\partial m_d^r}$, and \uplus denotes summing over the matrix. The value of $a_d^{n,r}$ indicates the importance of the d -th feature map m_d^r of r -th layer for the prediction class probability \bar{y}_n . The larger $a_d^{n,r}$, the more critical the feature map is.

Similarly, for the linear layer, there exists a value $a_d^{n,s}$ indicating the importance of the d -th output value v_d^s of the s -th linear layer for the predicted probability \bar{y}_n . The calculation for $a_d^{n,s}$ is given as follows:

$$a_d^{n,s} = \left| \frac{\partial \bar{y}_n}{\partial v_d^s} \right|^+. \quad (6)$$

Fig. 2 shows the statistical correlation diagram between all classes and the convolutional filters (a) / linear filters (b) in 13-th convolution layer / 2-nd linear layer of VGG-16 ON CIFAR-10-A. For each class, we calculate the sum value $\sum_1^{100} a_d^{n,r} / \sum_1^{100} a_d^{n,s}$ for each convolutional / linear filter of 100 images. The prediction confidences of those 100 images are larger than 0.90. From Fig. 2, we can observe that each class is only correlated with sparse and specific convolutional / linear filters (bright color), while most convolutional / linear filters are not correlated (dark color). For each image, the convolutional / linear filters with high correlation are almost identical with the statistical high correlation filters in each layer of the classifier. In summary, each class is only correlated with sparse and specific filters in the CNN classifier, consistent with the parallel processing mechanism [11, 28] and subdivision [11]. Above discovery is the basic support for the following analysis and disassembling and assembling operation.

4.3 Layer Component Bridging

After obtaining the fixed feature maps / values in the convolutional / linear layers, the following step analyzes the relationship between the critical features and preceding / subsequent parameter layers, which will bridge the feature routes of any two adjacent layers.

For the relation between the preceding parameter layer and features, from Eqn.(1), we can see that, with the same input feature maps $\{m_1^{r-1}, m_2^{r-1}, \dots, m_{d^{r-1}}^{r-1}\}$, the different convolutional filter c_d^r determines values of the output feature maps $\{m_1^r, m_2^r, \dots, m_{d^r}^r\}$. Therefore, the importance of the feature map m_d^r is closely linked with the d -th convolutional filter c_d^r . Similarly, the importance of the feature value v_d^s is closely linked with the d -th linear filter e_d^s in the linear connection layers.

For the relation between the subsequent parameter layer and features, as shown in Fig. 1, a dot products between feature maps $\{m_d^r\}_{d=1}^{d^r}$ and kernels $\{k_d^r\}_{d=1}^{d^r}$ of each convolution filter is conducted in the $(r+1)$ -th layer. For an unimportant feature map m_d , the corresponding kernel k_d of each filter is supposed to be also unimportant for the specific class.

Overall, the forward analysis locates the relevant convolutional filters and removes irrelevant convolutional filters for the specific class, while the backward analysis removes the irrelevant kernels of each filter for the specific class, which bridges the feature route between the parameter components (filters or kernels) of two adjacent layers.

Table 1: The performance of model disassembling on CIFAR-10-A, CIFAR-100-A, and Tiny-ImageNet-A. ‘orig.’, ‘disa.’, and ‘ep.+1’ denote the accuracy of the original classifier, disassembled classifier, and disassembled classifier with another one-epoch fine-tune, respectively (All score are in %).

Dataset	disassembled class	SimpleNetV1			VGG-16			ResNet-50		
		orig.	disa.	ep.+1	orig.	disa.	ep.+1	orig.	disa.	ep.+1
CIFAR-10-A	0	93.90	100.00	100.00	95.40	100.00	100.00	94.50	100.00	100.00
	1	92.20	92.90	95.40	91.30	100.00	100.00	93.20	100.00	100.00
	0-2	93.93	50.33	94.03	94.13	79.40	96.99	93.80	42.27	93.83
	2-4	96.33	56.90	98.17	95.57	81.03	98.27	95.37	76.47	98.50
CIFAR-100-A	0	91.00	99.40	100.00	88.00	100.00	100.00	87.00	100.00	100.00
	1	88.00	100.00	100.00	86.00	100.00	100.00	87.00	100.00	100.00
	0-9	80.50	85.60	90.60	78.50	88.50	88.80	78.80	51.80	88.10
	10-49	79.83	80.55	81.15	77.58	79.35	79.00	78.75	73.73	79.53
Tiny-ImageNet-A	0	90.00	100.00	100.00	90.00	100.00	100.00	89.00	100.00	100.00
	1	66.00	100.00	100.00	64.00	100.00	100.00	65.00	100.00	100.00
	0-9	72.20	85.60	90.60	70.40	52.20	72.60	71.60	52.00	74.60
	10-49	82.00	72.25	77.00	66.40	63.35	72.45	68.6	65.80	73.10

Table 2: The performance of the assembled models for three CNN classifiers. ‘asse.’ denotes the accuracy of the assembled classifier (All score are in %).

Dataset	assembled class	SimpleNetV1			VGG-16			ResNet-50		
		orig.	asse.	ep.+1	orig.	asse.	ep.+1	orig.	asse.	ep.+1
CIFAR-10-A	A0, A4	93.05	66.80	96.60	93.35	93.70	97.45	93.85	50.00	93.50
	A0-1,A3-4	94.58	59.60	93.73	94.13	78.48	93.70	94.38	45.28	93.95
CIFAR-10-B	A0, B0	94.95	50.00	93.65	96.10	50.50	97.20	96.00	50.00	90.80
	A0-2, B3-4	94.86	30.62	93.06	94.50	49.68	93.28	94.36	20.00	93.04
CIFAR-100-A	A0,A49	89.50	93.00	95.50	87.00	99.00	98.00	87.00	50.00	66.00
	A0-9,A30-49	80.03	81.37	83.97	78.47	82.03	81.97	80.30	66.90	82.47
CIFAR-100-B	A0,B0	78.00	50.00	75.50	74.00	50.00	90.00	79.50	50.00	77.50
	A0-9,B20-39	79.43	76.13	82.53	74.00	76.33	79.83	79.24	34.73	80.03
Tiny-ImageNet-A	A0,A40	78.00	69.00	88.00	77.00	97.00	98.00	77.00	50.00	82.00
	A0-9,A30-49	69.33	71.33	73.67	66.60	64.87	70.47	67.80	48.20	72.30
Tiny-ImageNet-B	A0,B0	89.00	50.00	86.00	86.00	51.00	90.00	87.50	52.30	88.10
	A0-9,B20-39	69.40	55.40	70.00	68.07	51.93	68.07	70.50	51.60	71.50

5 CNN Model Assembling

In the model assembling phase, disassembled class-aware model components, which can be from the same or different models, are expected to be easily assembled into a new model without performance loss.

For the same model case, there are some filters (simultaneous bright channels) shared by different classes, as shown in Fig. 2. Therefore, when assembling components from the same model, the commonly shared components keep unchanged and only assemble the independent components of different classes.

For different model cases, we propose a simple alignment padding strategy to assemble class-aware components of different models through padding empty kernels for each convolutional / linear filter, which ensures that all filters in each layer have the same number of kernels. In this paper, we only investigate assembling different models with the isomorphic network architecture. As shown in Fig 1, for each layer, the disassembled filter $\{k_1^{r,c1}, k_2^{r,c1}, \dots, k_p^{r,c1}\}$ composed of p kernels for class $c1$ and filter $\{k_1^{r,c2}, k_2^{r,c2}, \dots, k_q^{r,c2}\}$ composed of q kernels for class $c2$ from different CNN classifiers are assembled into two new filters $\{0_1, 0_2, \dots, 0_q, k_{q+1}^{r,c1}, k_{q+2}^{r,c1}, \dots, k_{q+p}^{r,c1}\}$ and $\{k_1^{r,c2}, k_2^{r,c2}, \dots, k_q^{r,c2}, 0_{q+1}, 0_{q+2}, \dots, 0_{q+p}\}$ by padding zero kernels $\{0_x\}$ in the alignment position. The simple alignment padding strategy can be easily extended to multiple class-aware components, which should ensure that the alignment position is padded with zero kernels $\{0_x\}$. A new classifier will be obtained by assembling the class-aware components layer by layer with the alignment padding strategy. The newly assembled classifier can be directly used for classifying the target classes.

6 Experiments

6.1 Experimental Setting

Network and Dataset. The experiments adopt three CNN models (SimpleNetV1 [16], VGG-16 [42], ResNet-50 [17]) and three datasets (CIFAR-10 [22], CIFAR-100 [22], Tiny-ImageNet [23]). To perform the model assembling experiments, we split CIFAR-10 into two datasets for 5-classification, termed as CIFAR-10-A and CIFAR-10-B. In similar, CIFAR-100 and Tiny-ImageNet are split into two datasets for 50-classification and 100-classification, denoted as CIFAR-100-A, CIFAR-100-B, Tiny-ImageNet-A, and Tiny-ImageNet-B.

Parameter Setting. In the training stage, all the learning rates for three classifiers are set as $lr = 0.01$, and SGD is chosen as the optimizer with the parameters $momentum = 0.9$ and $T_{max} = 200$. The batch size for CIFAR-10(A, B), CIFAR-100(A, B), and Tiny-ImageNet(A, B) is 128, 128, and 32, respectively. The number of training epochs is 100 on CIFAR-10(A, B) and 200 on CIFAR-100(A, B) as well as Tiny-ImageNet(A, B). In the one-epoch fine-tuning stage, apart from $lr = 0.001$ on CIFAR-10(A, B), $lr = 0.0001$ is applied on the other datasets. In addition, the default disassembled layer is the penultimate layer(2-nd convolutional layer), and the threshold for distinguishing critical features is set as the mean value, which calculated separately from each layer.

6.2 Model Disassembling and Assembling Results

In this section, we conduct model disassembling and assembling experiments on the above three CNNs with the six divided datasets. The experimental results are reported as an average of three runs to ensure fairness. Before disassembling and assembling, the models are trained by feeding with the divided datasets.

Table 1 shows the model accuracy on CIFAR-10-A, CIFAR-100-A, and Tiny-ImageNet-A. ‘orig.’, ‘disa.’, and ‘ep.+1’ denote the accuracy of the original classifier, disassembled classifier, and disassembled classifier with another one-epoch fine-tune, respectively. In the experiment, three networks (SimpleNetV1, VGG-16, and ResNet-50) are disassembled to the second convolutional layer.

From Table 1, we can conclude that the disassembled models obtain improved accuracy for single-class disassembling tasks (‘0’ and ‘1’) and stay close to the original accuracy for multi-class disassembling tasks (‘0-2’, ‘2-4’, ‘0-9’, ‘10-49’), which verifies the feasibility of MDA-Task and the effectiveness of the proposed FRAT. Meanwhile, the accuracy of the disassembled model is generally higher after one-epoch fine-tune.

Model assembling can be conducted on both the same models and different models. Table 2 shows the performance of the assembled models with class-aware components from three models on the six divided datasets. It can be observed that the assembled models achieve considerable performance with the original models in both assembling settings (single class and multiple classes). Similarly, the performance can be further improved with one-epoch fine-tune.

6.3 Model Decision Route Visualization

The proposed MDA-Task framework reveals the feature delivery routes associated with different classes, thus can be used to visualize the model decision routes. For example, Fig. 3 depicts a schematic diagram of the decision routes for the VGG-16 partial structure on CIFAR-10-A, with class ‘dog’ and class ‘bird’. It is observed that there exists a coupling of routes corresponding to different classes, and the shallower layer shares a more complex coupling. For lack of space, the actual decision route diagram and corresponding descriptions are provided in the supplementary material.

6.4 Model Diagnosing and Treating

In further, we can apply the proposed FRAT on model diagnosing and treating tasks in two steps. The decision route related to each class in the model is firstly extracted, and the routes for low-confidence or incorrect classes can be corrected to improve model performance. Table 3 reports the performance improvement via FRAT-based model diagnosing and treating in comparison with Model Doctor (MD) [13], where we can see that the proposed method achieves higher optimized accuracy than

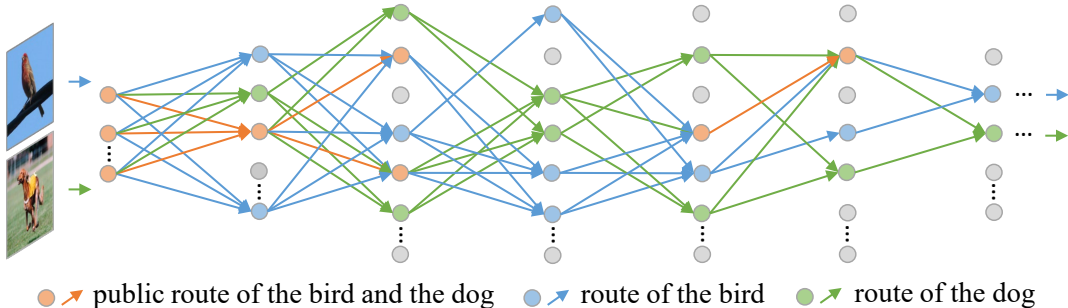


Figure 3: The schematic diagram of the decision routes for the VGG-16 partial structure on CIFAR-10-A, with class ‘dog’ and class ‘bird’.

Table 3: The performance comparison of Model Doctor [13] and our proposed method on deep model diagnosing and treating (All score are in %).

Dataset	SimplenetV1			VGG-16			ResNet-50		
	orig.	MD [13]	Our	orig.	MD [13]	Our	orig.	MD [13]	Our
CIFAR-10-A	95.02	95.58	95.73	94.76	95.02	95.83	94.76	95.11	95.92
CIFAR-100-A	79.96	80.55	81.97	77.76	78.87	80.33	78.60	79.08	80.36
Tiny-ImageNet-A	68.58	69.31	70.84	65.28	67.14	68.25	64.30	66.80	67.46

Table 4: The performance on the model compression task. ‘orig.’ and ‘comp.’ denote the accuracy of original classifier and compressed classifier. ‘size⁻’ denotes the compressed model size. (All scores are in %).

Dataset	SimpleNetV1			VGG-16			ResNet-50		
	orig.	comp.	size ⁻	orig.	comp.	size ⁻	orig.	comp.	size ⁻
CIFAR-10-A	95.02	67.82	14.84	94.76	94.68	23.03	94.76	49.40	29.98
CIFAR-100-A	79.96	79.50	21.53	77.76	77.54	2.85	78.60	72.02	1.89
Tiny-ImageNet-A	68.58	66.74	1.22	65.28	62.24	8.34	64.30	55.53	4.43

MD [13]. This also verifies that the proposed method can attribute more accurate class-aware features and feature routes for the specific class.

6.5 Model Compression

In addition, the MDA-Task framework can be used for model compression to improve the speed of model inference. After obtaining the decision route for each class by FRAT, the parameters outside the decision route can be eliminated. Table 4 shows the model compression performance of the three models on three datasets. The compression rates are more significant for datasets with a small number of classes, which may be explained that the coupling level and decision routes are complicated with more classes.

6.6 Application on Other Tasks

In addition to the above tasks, MDA-Task and the proposed model disassembling and assembling framework can also be used for knowledge distillation, transfer learning, incremental learning, etc.

Due to space limitations, more experiments are given in the supplementary material.

6.7 Ablation Study

This section conducts the ablation study of the disassembling layer number, strategies for processing derivatives, and the threshold for filtering high and low association feature maps.

Disassembled layer number.

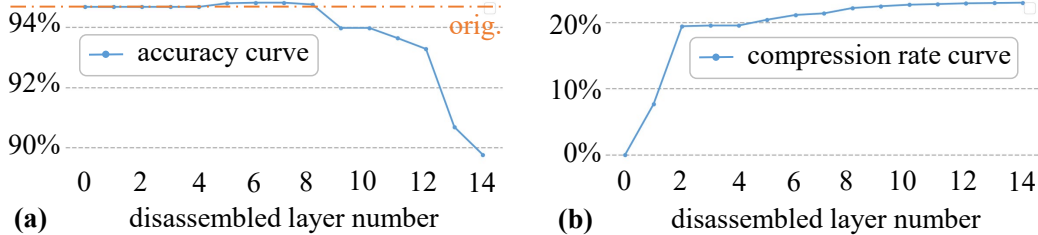


Figure 4: Ablation study on the disassembled depth of the model layer. Model accuracy (a) and compression rate (b) of disassembling layer from deep to shallow. ‘0’ denotes the last linear layer, and ‘14’ denotes the first convolutional layer on VGG-16.

Table 5: Ablation study on the choice of derivative. ‘ $size^-$ ’ denotes the compressed model size (All scores are in %).

VGG-16	positive	negative	absolute
(accuracy, $size^-$)	(91.34, 22.74)	(32.30, 36.54)	(87.76, 29.80)

Based on VGG16 and CIFAR-10-A, we conduct ablation experiments on the disassembled depth of the model layer from deep to shallow. Fig 4(a) shows the accuracy curve along with the increased disassembled layer number. The performance of the model tends to decrease slightly as the model is disassembled with shallower layers. The possible reason is that the shallow layer of the model contains more low-level semantic features that are not yet completely separated, and the model coupling level is relatively high, where disassembling by FRAT will cause parameter loss and affect the model performance. Fig 4(b) shows the compression rates for disassembling with different layers. It can be seen that as more layers are disassembled, the compression rate of the model tends to rise.

Choice of derivative.

In further, we investigate different treatment strategies for the first-order derivatives calculated in Eqn. (1). Table 5 shows the performance of model compression on VGG16 and CIFAR-10-A when different strategies are applied, where applying negative values of the first-order derivatives results in the worst compression performance, followed by adopting the absolute values and using the positive values achieves the best result. The possible reason is that in the feature attribution stage, the negative value of the first-order derivative of the class \bar{y}_n on the feature map m_d^r actually reflects the noise features, whereas the positive value reflects the effective features.

Threshold value.

Finally, we experiment on the thresholds for filtering high and low association feature maps in Fig. 2(a) and feature values in Fig. 2(b). With the increase of the threshold value, the compression rate of the model increases, and the accuracy rate decreases. On the contrary, with the threshold value decreasing, the compression rate of the model decreases and the accuracy rate increases. In fact, as the threshold increases, fewer important parameters will be retained, resulting in a model with a simplified structure and inferior performance. Therefore, using the ‘mean value’ as the threshold is most effective when considering both the model compression rate and the performance.

6.8 Limitation and Future Work

In Fig. 5(a), it reveals that the proposed disassembling and assembling framework is unable to achieve sufficient disassembling of different classes at a shallower level, leading to degradation of the model performance. Besides, more complex networks, such as GoogLeNet [46] or InceptionNet [20] containing Inception structures, require further adaptation for model assembling. In this paper, we only investigate the MDA-Task on CNN classifier with the isomorphic network architecture. In the future, we will explore the universality and generalization of MDA-Task with more model architectures (isomorphic or heterogeneous) and model types (CNN, GCN, GNN, RNN, Transformer) on a wide range of tasks (segmentation, detection, tracking, and so on). Of course, more accurate feature attribution techniques and more practical model disassembling and assembling methods are both focuses of our future research.

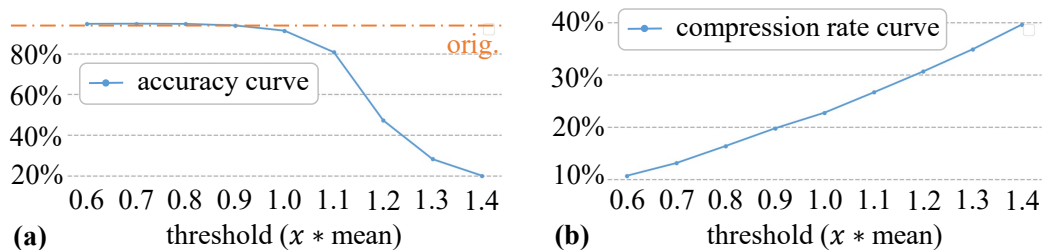


Figure 5: Ablation study on the threshold. (a) Model accuracy with different thresholds ($x * \text{mean}$). (b) Model compression rate with different thresholds ($x * \text{mean}$). ‘orig.’ denotes the accuracy of the original classifier.

7 Conclusion

In this paper, we introduce a new MDA-Task, in aim to disassemble and assemble deep models without performance loss like playing LEGO toys, which is inspired by the subdivision of visual system [28]. The MDA-Task is applicable for existing deep learning models such as CNN, GCN, GNN, RNN, Transformer, et al. We focus on investigating the MDA-Task on the CNN classifiers in this paper. The essence of disassembling CNN classifier is to discover the inherent feature route associated with the specific class, which is split into two steps: critical feature attribution and bridging the route between two adjacent layers. In disassembling stage, the feature route attribution technique (FRAT) is proposed for attributing the critical features in each layer and bridging the feature route between the two adjacent layers. The whole feature route of a CNN classifier will be built based on the discovered feature routes between preceding and subsequent parameter layers. In the assembling stage, a simple alignment padding strategy is devised for assembling class-aware components of the same or different CNN classifiers. Extensive experiments show that assembled new classifier can achieve close even better performance than the original classifier. What’s more, we also verified the broad application of MDA-Task on various tasks, such as decision route visualization, model compression, knowledge distillation, and so on.

References

- [1] Ancona, M., Ceolini, E., ztireli, C., Gross, M.: Towards better understanding of gradient-based attribution methods for deep neural networks. In: ICLR (2018)
- [2] Bach, S., Binder, A., Montavon, G., Klauschen, F., Müller, K.R., Samek, W.: On pixel-wise explanations for non-linear classifier decisions by layer-wise relevance propagation. PLOS ONE **10**(7), 130140 (2015)
- [3] Baehrens, D., Schroeter, T., Harmeling, S., Kawanabe, M., Hansen, K., Müller, K.R.: How to explain individual classification decisions. Journal of Machine Learning Research **11**(61), 1803–1831 (2010)
- [4] Bastani, O., Kim, C., Bastani, H.: Interpretability via model extraction. arXiv preprint arXiv:1706.09773 (2017)
- [5] Belouadah, E., Popescu, A.: I12m: Class incremental learning with dual memory. In: Proceedings of the IEEE/CVF International Conference on Computer Vision. pp. 583–592 (2019)
- [6] Chaudhry, A., Dokania, P.K., Ajanthan, T., Torr, P.H.: Riemannian walk for incremental learning: Understanding forgetting and intransigence. In: Proceedings of the European Conference on Computer Vision (ECCV). pp. 532–547 (2018)
- [7] Chen, Y., Mao, F., Song, J., Wang, X., Wang, H., Song, M.: Self-born wiring for neural trees. In: Proceedings of the IEEE/CVF International Conference on Computer Vision. pp. 5047–5056 (2021)
- [8] Desai, S., Ramaswamy, H.G.: Ablation-cam: Visual explanations for deep convolutional network via gradient-free localization. In: WACV. pp. 983–991 (2020)
- [9] Ding, X., Ding, G., Guo, Y., Han, J.: Centripetal sgd for pruning very deep convolutional networks with complicated structure. In: Proceedings of the IEEE Conference on Computer Vision and Pattern Recognition. pp. 4943–4953 (2019)
- [10] Erhan, D., Bengio, Y., Courville, A., Vincent, P.: Visualizing higher-layer features of a deep network. University of Montreal (2009)
- [11] Essen, D.V., Deyoe, E.A.: Concurrent processing in the primate visual cortex. Cognitive Neuroence pp. 383–400 (1995)

- [12] Feng, Y., Wu, F., Shao, X., Wang, Y., Zhou, X.: Joint 3d face reconstruction and dense alignment with position map regression network. In: ECCV. pp. 557–574 (2018)
- [13] Feng, Z., Hu, J., Wu, S., Yu, X., Song, J., Song, M.: Model doctor: A simple gradient aggregation strategy for diagnosing and treating cnn classifiers. AAAI (2022)
- [14] Guidotti, R., Monreale, A., Ruggieri, S., Pedreschi, D., Turini, F., Giannotti, F.: Local rule-based explanations of black box decision systems. arXiv preprint arXiv:1805.10820 (2018)
- [15] Guo, W., Mu, D., Xu, J., Su, P., Wang, G., Xing, X.: Lemna: Explaining deep learning based security applications. In: proceedings of the 2018 ACM SIGSAC conference on computer and communications security. pp. 364–379 (2018)
- [16] HasanPour, S.H., Rouhani, M., Fayyaz, M., Sabokrou, M.: Lets keep it simple, using simple architectures to outperform deeper and more complex architectures. arXiv (2016)
- [17] He, K., Zhang, X., Ren, S., Sun, J.: Deep residual learning for image recognition. In: CVPR. pp. 770–778 (2016)
- [18] Hou, S., Pan, X., Loy, C.C., Wang, Z., Lin, D.: Learning a unified classifier incrementally via rebalancing. In: Proceedings of the IEEE/CVF Conference on Computer Vision and Pattern Recognition. pp. 831–839 (2019)
- [19] Hubel, D.H., Wiesel, T.N.: Receptive fields, binocular interaction and functional architecture in the cat’s visual cortex. *The Journal of physiology* **160**(1), 106 (1962)
- [20] Ioffe, S., Szegedy, C.: Batch normalization: Accelerating deep network training by reducing internal covariate shift. In: International conference on machine learning. pp. 448–456. PMLR (2015)
- [21] Kindermans, P.J., Schütt, K., Müller, K.R., Döhne, S.: Investigating the influence of noise and distractors on the interpretation of neural networks. arXiv preprint arXiv:1611.07270 (2016)
- [22] Krizhevsky, A., Hinton, G., et al.: Learning multiple layers of features from tiny images (2009)
- [23] Le, Y., Yang, X.: Tiny imagenet visual recognition challenge. *CS 231N* **7**(7), 3 (2015)
- [24] LeCun, Y., Bottou, L., Bengio, Y., Haffner, P.: Gradient-based learning applied to document recognition. *Proceedings of the IEEE* **86**(11), 2278–2324 (1998)
- [25] Lei, J., Wang, Z., Feng, Z., Song, M., Bu, J.: Understanding the prediction process of deep networks by forests. In: BigMM. pp. 1–7 (2018)
- [26] Lengerich, B.J., Konam, S., Xing, E.P., Rosenthal, S., Veloso, M.M.: Visual explanations for convolutional neural networks via input resampling. arXiv preprint arXiv:1707.09641 (2017)
- [27] Li, Y., Lin, S., Zhang, B., Liu, J., Doermann, D., Wu, Y., Huang, F., Ji, R.: Exploiting kernel sparsity and entropy for interpretable cnn compression. In: Proceedings of the IEEE Conference on Computer Vision and Pattern Recognition (CVPR) (2019)
- [28] Livingstone, M.S., Hubel, D.H.: Psychophysical evidence for separate channels for the perception of form, color, movement, and depth. *Journal of Neuroscience* **7**(11), 3416–3468 (1987)
- [29] Mahendran, A., Vedaldi, A.: Understanding deep image representations by inverting them. CVPR (2015)
- [30] Naidu, R., Michael, J.: Ss-cam: Smoothed score-cam for sharper visual feature localization. arXiv preprint arXiv:2006.14255 (2020)
- [31] Nguyen, A., Yosinski, J., Clune, J.: Multifaceted feature visualization: Uncovering the different types of features learned by each neuron in deep neural networks. CVPR (2016)
- [32] Nguyen, A., Dosovitskiy, A., Yosinski, J., Brox, T., Clune, J.: Synthesizing the preferred inputs for neurons in neural networks via deep generator networks. NeurIPS (2016)
- [33] Rahman Amik, F., Tasin, A.I., Ahmed, S., Lutfe Elahi, M., Mohammed, N.: Dynamic rectification knowledge distillation. arXiv e-prints pp. arXiv–2201 (2022)
- [34] Ribeiro, M.T., Singh, S., Guestrin, C.: Nothing else matters: Model-agnostic explanations by identifying prediction invariance. arXiv preprint arXiv:1611.05817 (2016)
- [35] Ribeiro, M.T., Singh, S., Guestrin, C.: "why should i trust you?": Explaining the predictions of any classifier. ACM SIGKDD Int Conf on Knowledge Discovery and Data Mining (2016)
- [36] Ribeiro, M.T., Singh, S., Guestrin, C.: Anchors: High-precision model-agnostic explanations. AAAI (2018)
- [37] Shen, C., Wang, X., Song, J., Sun, L., Song, M.: Amalgamating knowledge towards comprehensive classification. In: Proceedings of the AAAI Conference on Artificial Intelligence. vol. 33, pp. 3068–3075 (2019)
- [38] Shrikumar, A., Greenside, P., Kundaje, A.: Learning important features through propagating activation differences. In: ICML (2017)

- [39] Shrikumar, A., Greenside, P., Shcherbina, A., Kundaje, A.: Not just a black box: Learning important features through propagating activation differences. arXiv preprint arXiv:1605.01713 (2016)
- [40] Simonyan, K., Vedaldi, A., Zisserman, A.: Deep inside convolutional networks: Visualising image classification models and saliency maps. *Computer Science* (2013)
- [41] Simonyan, K., Vedaldi, A., Zisserman, A.: Deep inside convolutional networks: Visualising image classification models and saliency maps. In: *ICLR Workshop* (2013)
- [42] Simonyan, K., Zisserman, A.: Very deep convolutional networks for large-scale image recognition. arXiv preprint arXiv:1409.1556 (2014)
- [43] Song, J., Chen, Y., Wang, X., Shen, C., Song, M.: Deep model transferability from attribution maps. In: *NeurIPS*. vol. 32, pp. 6179–6189 (2019)
- [44] Sterling, B.: Inceptionism: going deeper into neural networks. *Google Research Blog* (2011)
- [45] Sundararajan, M., Taly, A., Yan, Q.: Axiomatic attribution for deep networks. In: *ICML* (2017)
- [46] Szegedy, C., Liu, W., Jia, Y., Sermanet, P., Reed, S., Anguelov, D., Erhan, D., Vanhoucke, V., Rabinovich, A.: Going deeper with convolutions. In: *Proceedings of the IEEE conference on computer vision and pattern recognition*. pp. 1–9 (2015)
- [47] Treisman, Anne., M.: Selective attention in man. *Br Med Bull* **20**(1), 12–16 (1963)
- [48] Wang, H., Wang, Z., Du, M., Yang, F., Zhang, Z., Ding, S., Mardziel, P., Hu, X.: Score-cam: Score-weighted visual explanations for convolutional neural networks. In: *CVPR Workshops*. pp. 111–119 (2020)
- [49] Wang, J., Zhang, P., He, Q., Li, Y., Hu, Y.: Revisiting label smoothing regularization with knowledge distillation. *Applied Sciences* **11**(10), 4699 (2021)
- [50] Xue, M., Song, J., Sun, L., Song, M.: Tree-like branching network for multi-class classification. In: *International Conference on Intelligent Computing & Optimization*. pp. 175–184. Springer (2021)
- [51] Zeiler, M.D., Fergus, R.: Visualizing and understanding convolutional networks. In: *ECCV* (2014)
- [52] Zhou, B., Khosla, A., Lapedriza, A., Oliva, A., Torralba, A.: Learning deep features for discriminative localization. *IEEE Computer Society* (2016)
- [53] Zhou, J., Troyanskaya, O.G.: Predicting effects of noncoding variants with deep learning–based sequence model. *Nature Methods* **12**(10), 931–934 (2015)
- [54] Zintgraf, L.M., Cohen, T.S., Adel, T., Welling, M.: Visualizing deep neural network decisions: Prediction difference analysis. In: *ICLR* (2017)

A Appendix

In this part, we provide the *source code* and more applications on model decision route visualization, model compression, knowledge distillation, incremental learning, and transfer learning.

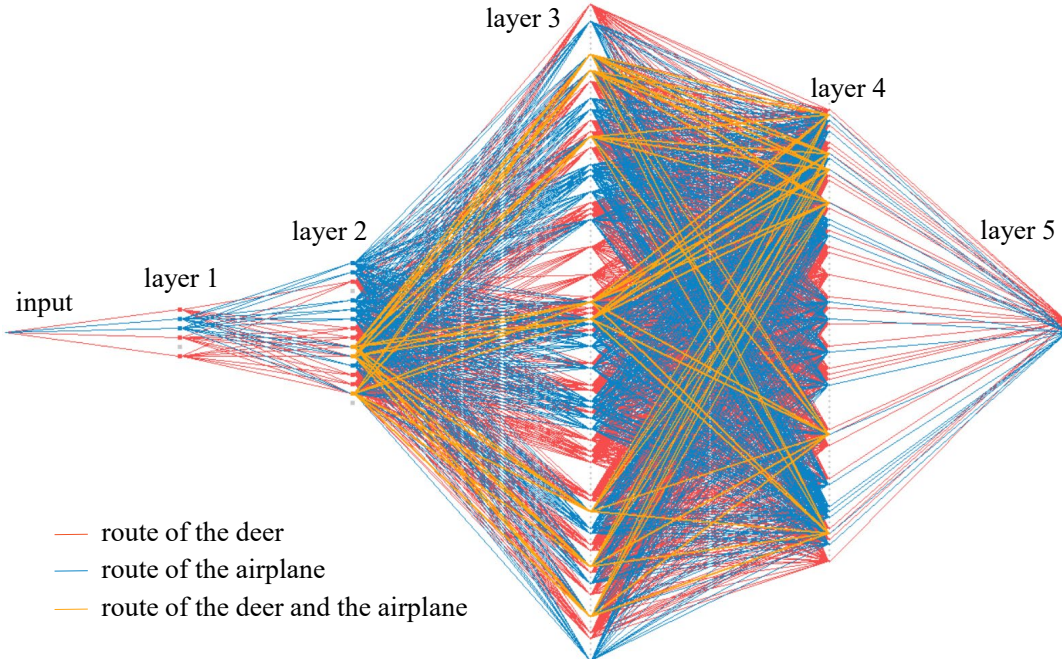


Figure 6: The decision route of the LeNet-5.

A.1 Model Decision Route Visualization

As described in the submitted manuscript, the proposed method can be used to visualize the decision route of CNN classifiers. In this section, we take the LeNet-5 [24], including two-layer convolution and three-layer linear, as an example to clearly demonstrate the decision path for specific classes, as shown in Fig. 6. As we demonstrate with the schematic diagram in the submitted manuscript, each class has its own decision route, but it’s not completely independent.

For the deer and airplane, the number of share convolution components (convolutional kernels or neurons) are summarized as follows: layer1: 0%, layer2: 15.38%, layer3: 13.11%, layer4: 11.54%, and layer5: 0%. In the 2-nd convolution layer and 3-rd linear layer, two classes have many shared convolutional kernels and linear neurons. The reason is that those low-level convolutional kernels are responsible for processing color, form, texture, edge features, and so on, which is consistent with some existing research [10, 29, 31, 32, 40, 44] and biological visual information processing mechanism [11, 28, 47]. In the last layer, connections between different neurons are sparse and fixed, which is consistent with the fact that class-aware features occur in the high level of CNN. In conclusion, the visualization of the model decision route for the specific class is a benefit for investigating the underlying mechanism of the CNN classifier and debugging the CNN classifier.

A.2 Model Compression

In this section, we give detailed results of model compression by our MDA-Task framework and correct some experimental data as shown in Table 6. Some comparative experiments with SOTA methods including KSE [27], C_SGD [9], are shown in Table 7, where KSE and C_SGD are both pruning-based methods. From Table 7, we can see that our method achieves close accuracy with KSE and C_SGD, lower FLOPs score than other methods, which means that the proposed method can find more accurate and compact parameters related to specific parameters.

Table 6: The performance on the model compression task. D_1 , D_2 , and D_3 denote the datasets CIFAR-10-A, CIFAR-100-A, and Tiny-ImageNet-A, respectively. ‘orig.’, ‘comp.’, and ‘ep.+1’ denote the accuracy of the original classifier, compressed classifier, and compressed classifier with another one-epoch fine-tune, respectively. ‘para.’ denotes the compression ratio. ‘FLOPs.’ denotes the acceleration ratio. (All scores are in %).

Network	Dataset	orig.	comp.	ep.+1	para.	FLOPs
SimpleNetV1	D_1	95.02	67.82	93.66	14.87	32.33
	D_2	79.96	79.50	79.84	21.62	24.23
	D_3	68.58	66.74	68.18	1.23	9.84
VGG-16	D_1	94.68	89.76	94.36	23.04	13.36
	D_2	77.76	77.54	77.52	2.85	0.67
	D_3	65.28	62.24	64.44	8.34	5.14
ResNet-50	D_1	94.76	49.40	89.58	30.05	34.74
	D_2	78.60	72.02	77.56	1.89	7.27
	D_3	64.30	55.53	63.82	6.13	5.21

Table 7: The model compression performance comparison of different methods on CIFAR-10-A with VGG-16. ‘orig.’ and ‘comp.’ denote the accuracy of the original classifier and compressed classifier after one-epoch fine-tuning. ‘vari.’, ‘para.’, and ‘FLOPs’ denote the variation of the accuracy, the compression ratio, the acceleration ratio, respectively. (All scores are in %). C_SGD lacks the ‘para.’ result in the original paper, so we do not provide it either.

Method	orig.	comp.	vari.	para.	FLOPs
KSE [27]	94.68	94.24	-0.44	30.15	28.56
C_SGD [9]	94.68	94.53	-0.15	-	30.27
ours (MDA-Task)	94.68	94.36	-0.32	23.04	13.36

Table 8: The performance of knowledge distillation from single teacher to one student on CIFAR-100-A with VGG-16. ‘orig.’ denotes the accuracy of the original classifier. ‘ours’ denotes the accuracy of the student model by our MDA-Task framework (All scores are in %).

Dataset	single teacher	accuracy			
		orig.	LSR [49]	DR-KD [33]	ours
CIFAR-100-A (teacher)	A0-9	78.50	81.10	82.25	88.40
	A10-49	77.58	80.83	82.12	79.00

Table 9: The performance of knowledge distillation from multiple teachers to one student on CIFAR-100 (A, B) with VGG-16. ‘orig.’ denotes the accuracy of the original classifier. ‘ours’ denotes the accuracy of the student model by our MDA-Task framework.

Dataset	multiple teachers	accuracy		
		orig.	AK [37]	ours
CIFAR-100-A (teacher 1)	A0, B0	74.00	76.25	90.00
	A0-9, B0-9	76.35	77.24	82.10
CIFAR-100-B (teacher 2)	A0-9, B20-39	77.58	78.41	79.83
	A0-49, B0-49	78.13	78.67	68.02

A.3 Knowledge Distillation

In this section, the proposed method is compared with two kinds of knowledge distillation methods: single teacher to one student and multiple teachers to one student (also called knowledge aggregation).

As we can see from table 8, the model’s accuracy distilled based on our method is higher than the teacher’s. What’s more, we compared several SOTA methods on knowledge distillation, including LSR [49], DR-KD [33]. It is evident that when distilling a few classes, our method exceeds SOTA methods, and when distilling most classes, our method performs the worst.

Table 10: The performance of incremental six tasks on CIFAR-100. ‘orig.’, ‘new.’, and ‘avg.’ denote the accuracy of the original task classifier, the average accuracy of the newly added classes, and the average accuracy of all combined classes, respectively (All scores are in %).

Network	accuracy	task-0	task-1	task-2	task	task-4	task-5
SimpleNetV1	orig.	79.96	79.38	79.33	79.99	79.71	80.26
	new.	79.84	71.40	76.70	73.30	68.90	75.00
	avg.	79.84	76.22	74.90	73.03	71.26	70.41
VGG-16	orig.	77.76	77.17	77.56	78.03	77.62	78.13
	new.	77.52	64.70	73.00	71.20	62.50	73.20
	avg.	77.42	72.93	71.96	70.46	68.38	68.02
ResNet-50	orig.	78.60	78.08	78.67	79.24	79.18	79.69
	new.	77.56	70.30	76.30	73.10	69.60	73.60
	avg.	77.56	74.48	73.76	71.66	70.27	69.50

Table 11: The performance of some SOTA incremental learning methods on CIFAR-100 with VGG-16. ‘new.’ and ‘avg.’ denote the average accuracy of the newly added classes and the average accuracy of all combined classes, respectively (All scores are in%).

Method	accuracy	task-0	task-1	task-2	task-3	task-4	task-5
IL2M [5]	orig.	-	-	-	-	-	-
	new.	73.60	82.80	85.80	86.90	88.90	82.60
	avg.	73.60	77.00	77.60	76.50	77.30	76.10
Riemannian Walk [6]	orig.	-	-	-	-	-	-
	new.	70.70	85.10	85.10	87.60	87.70	87.00
	avg.	70.70	65.10	61.20	57.80	57.9	50.7
Rebalancing [18]	orig.	-	-	-	-	-	-
	new.	63.90	78.30	77.10	81.60	80.70	80.20
	avg.	63.90	70.30	70.90	71.80	69.70	68.00

The knowledge distillation from multiple teachers to one student is based on an isomorphic network. We compared our method with the SOTA method AK [37] as shown in Table 9. As we can see, the performance of our method exceeds AK [37] in most cases, but when the number of distillation classes increases, the performance becomes worse. The possible reason is that when there are more classes, the more coupled the model parameters are, and the more difficult to disassemble it.

A.4 Incremental Learning

One of the critical applications of our MDA-Task framework is incremental learning. Specifically, we train isomorphic networks in the different datasets composed of different classes. Then we implement incremental learning by combining one model with the model disassembled from the other model.

In this section, we provide some detailed experimental results on CIFAR-100 with three CNN classifiers in Table 10, and make a comparison with some SOTA methods, including IL2M[5], Riemannian Walk[6] and Rebalancing[18] as shown in Table 11. All processes of incremental learning in tables start from training on CIFAR-100-A and add ten novel classes respectively in the following tasks.

Table 10 shows the incremental learning performance of the proposed method with three mainstream CNN networks, where we can see that the proposed method achieves and ascends original scores. The possible reason is that newly added classes are beneficial for original classes to learn basic features. Meanwhile, a large number of unrelated parameters also disturb the classification performance of newly added classes, which leads to the descending new accuracy scores and descending average accuracy scores. Unequal training time for original and new classes is also a possible reason. Table 11 shows some SOTA methods on incremental learning. Apparently, the performance of our method is close to and even higher than some SOTA methods.

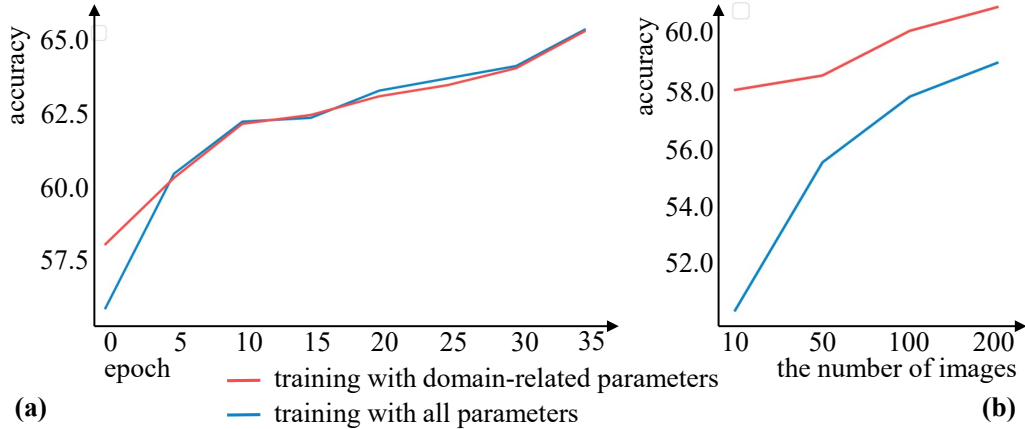


Figure 7: The performance of transfer learning from RGB images to grayscale images on randomly selected classes of Tiny-ImageNet. (a) Model accuracy with different epoch. (b) Model accuracy with different number of images.

A.5 Transfer Learning

We can also extend our MDA-Task framework in transfer learning, and we performed transfer experiments from RGB images to grayscale images on some randomly selected classes from Tiny-ImageNet. The essence of our method to improve the performance of transfer learning is to discover the class-related parameters and only train the class-independent (domain-related) parameters. We conduct a standard transfer experiment with all model parameters as a comparison.

As shown in Fig. 7(a), the transferred model guided by MDA-Task has higher accuracy in the first five training epochs. Then in the following training, the accuracy tendencies of the two methods are almost identical, which demonstrates our method can help the transferred model converge quickly. What's more, from Fig. 7(b), we can see that our method can achieve higher accuracy under the condition of limited images numbers.